ACS Catalysis

Research Article

pubs.acs.org/acscatalysis

The Alpha–Bet(a) of Salty Glucose Pyrolysis: Computational Investigations Reveal Carbohydrate Pyrolysis Catalytic Action by Sodium Ions

Heather B. Mayes,[†] Michael W. Nolte,[‡] Gregg T. Beckham,[§] Brent H. Shanks,*[,‡,∥] and Linda J. Broadbelt*[,†]

[†]Department of Chemical and Biological Engineering, Northwestern University, Evanston, Illinois 60208, United States

[‡]Department of Chemical and Biological Engineering, Iowa State University, Ames, Iowa 50011, United States

[§]National Bioenergy Center, National Renewable Energy Laboratory, Golden, Colorado 80401, United States

[∥]Center for Biorenewable Chemicals (CBiRC), Iowa State University, Ames, Iowa 50011, United States

Supporting Information

ABSTRACT: Biomass pyrolysis is a promising technology for the production of renewable fuels and chemicals from nonfood biomass. Given the potential of pyrolysis as a viable, cost-effective biomass deconstruction method, there is active interest in understanding the chemical transformations at the heart of the technology. It has long been known that the presence of alkali- and alkaline-earth-metal ions in biomass, such as Na^+, significantly alters product yields of biomass pyrolysis, but the mechanism behind this effect has not been elucidated. In this work, we employ density functional theory (DFT) to reveal the stereoelectronic basis of the effect of sodium ions on several key glucose thermal decomposition reactions, such as the formation of levoglucosan and 5-hydroxymethylfurfural (5-HMF). β-D-Glucose is of interest for pyrolysis, as it is the monomer of cellulose and a key intermediate in cellulose pyrolysis. α-D-Glucose is included in this study, as the two anomers can readily interconvert under pyrolysis conditions. The computational results are consistent with the experimental results for α- and β-D-glucose pyrolysis with NaCl, which demonstrate that the products are the same as those produced in neat pyrolysis, but with differing relative yields. We find that the sodium ion changes the reaction rate coefficients to varying degrees, with approximately 70% of the reactions in this study catalyzed by Na^+, approximately 25% inhibited by Na^+, and the remainder showing virtually no effect on the rate coefficient. The variations in how the ion modifies the rate coefficient reflect how the particular stereochemistry of the transition state interacts with the ion. The sodium ions have a more subtle effect on reactant electronic structure. The results of this study provide a molecular-level understanding of how naturally occurring salts act as catalysts in biomass pyrolysis.

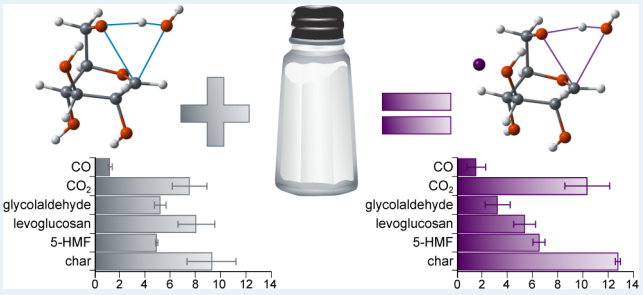

KEYWORDS: *biomass, cellulose, biofuels, 5-HMF, kinetics, dehydration, transition-state stabilization, inorganic salts*

1. INTRODUCTION

Terrestrial plant biomass is an abundant source of renewable carbon available to produce chemicals and energy-dense liquid fuels.[1−6] Fast pyrolysis is a promising technology for converting plant biomass into liquid bio-oil, which can be directly used to power turbines or upgraded to provide platform chemicals and drop-in liquid transportation fuels.[4,7−9] A current drawback to pyrolysis is the diverse product distribution that can significantly vary due to differences in feed and operating conditions, and an inability to predict the product distribution, thereby impeding efficient process design.[10−14] Cellulose, a homopolymer of β-D-glucose, is the most abundant component of plant biomass, and unlike the other major biomass components, hemicellulose and lignin, it has a highly regular structure.[3] Initial efforts to create predictive models for product yields from cellulose pyrolysis date to the 1970s, when Broido, Shafizadeh, and co-workers hypothesized simple kinetic models of cellulose pyrolysis.[15,16] These models and subsequent updates[17−19] empirically fit experimental results to a limited number of lumped components and kinetic parameters. Such empirical models do not require mechanistic knowledge of the process chemistry and provide a computationally inexpensive estimate of product yields, but they provide limited information about product speciation, are valid only in the range of conditions used in the model training data, and are not extendable. Recent experimental efforts have determined detailed product yields of neat cellulose pyrolysis,[20−22] and experimental and computational studies have provided

Received: August 3, 2014
Revised: October 16, 2014
Published: November 13, 2014

information on the elementary reaction mechanisms.[23−28] These studies and others allowed Vinu and Broadbelt to build the first mechanistic model of cellulose pyrolysis, accurately predicting cellulose pyrolysis product yields over a variety of process conditions.[29] Furthermore, their model provides information that is inaccessible directly from experiment, such as the temporal evolution of species, dominant reaction pathways for the formation of key products, and evidence that glucose is an important intermediate.

Unlike empirical models, mechanistic models are extensible. Additional chemical reactions can be added to the existing framework of the mechanistic model of neat cellulose pyrolysis to benefit from new discoveries[30,31] and to include additional components of plant biomass. This work provides required kinetic data to extend mechanistic models of glucose-based carbohydrate pyrolysis to include the effects of inorganic salts. Such salts are naturally present in biomass, and even small amounts have a profound effect on the pyrolysis product distribution.[32−44] Sodium is one of several common metals found in biomass, and its effect on the product distribution from cellulose pyrolysis is similar to that of other alkali and alkaline-earth metals.[41,42,45] Removing inorganic salts from biomass feedstocks requires additional processing and adds cost,[46] and even small amounts of residual salts could drastically change the yield distribution. Detailed product yields for cellulose fast pyrolysis at 500 °C have shown that the presence of NaCl decreases the yield of levoglucosan while increasing the yield of water, char, and several low-molecular-weight species such as carbon dioxide.[36,41,42,45,47,48] Interestingly, the product species do not change, only their relative amounts, suggesting that salts alter relative rates for different pyrolysis reactions and increase the overall rate of reaction.

While the effect of inorganic salts on cellulose pyrolysis reactions is well-known, the physical basis for the differences and quantitative effect on reactions has received little study to date.[49] Early proposals suggested that salts coordinate with ionic intermediates of a heterolytic cellulose pyrolysis mechanism,[20,35,44,45,50] although a concerted mechanism has recently been shown to be more likely[26] and has been shown to provide results consistent with experiment.[29−31] Yu et al. suggested that ions such as Mg^{2+} and Na^{+} coordinate with the ring oxygen, facilitating ring-opening reactions.[44] Saddawi et al. used DFT to optimize several model reactant conformations with a potassium ion and speculated that a sodium or potassium ion could complex with a pyrolysis reactant or intermediate to stabilize a particular conformation that facilitates ring opening.[51] Nimlos et al. performed electronic structure calculations to study the effect of a sodium ion on ethanol dehydration in the gas phase.[52] They investigated the transition states as well as the reactants and reported a lowering of the activation energy from 67.4 to 60.0 kcal/mol and a rate coefficient approximately 3 times higher in the presence of Na^{+}.

In the present study, we explore the effect of sodium ions on several key glucose pyrolysis reactions and compare the kinetic parameters to our previous results with neat glucose.[53] As noted in our previous study, glucose is an excellent choice for electronic structure calculations to model cellulose pyrolysis reactions, because this monomer of cellulose is also an important cellulose pyrolysis intermediate.[53] Direct, experimental evidence of intermediates is difficult because of their fleeting nature. However, experimental evidence corroborating glucose as an intermediate includes identification of glucose in the product slate of cellulose pyrolysis.[32,37,54,55] Theoretical modeling[29−31] has provided a strong basis to suggest that many of the low-molecular-weight species evolve from glucose, providing a chemistry-based rationale behind why all products formed from glucose pyrolysis are observed in the pyrolysis products of glucose-based carbohydrates including cellulose.[20,56,57] Several previous studies have found that the cation of an inorganic salt such as NaCl interacts more closely with carbohydrates than do anions such as Cl^{-},[47,58,59] justifying continued focus on the effects of the cation on carbohydrate pyrolysis reactions. Our previous simulation work indicates that cations directly interact with the nucleophilic oxygens,[58] which are central in the dominant reactions in carbohydrate pyrolysis, dehydration, and isomerization.[23−25,29,30] In contrast, the counterion, Cl^{-}, was preferably located farther from the carbohydrate reaction centers, interacting instead with the partially positively charged hydrogen atoms.[58] These data indicate that the role of anions in carbohydrate pyrolysis may primarily lie in their affinity for binding with the cation, competing with cation−carbohydrate interactions, rather than directly affecting carbohydrate reaction kinetics.

The present work provides a valuable extension to the study by Nimlos et al.,[52] as the larger substrate offers multiple low-energy sites for interaction with the ion[58] in addition to multiple reaction sites.[53] We present experimental results for glucose pyrolysis in the presence of NaCl to determine the extent of its effect on pyrolysis of the monomer and to provide context for the DFT study. Capturing the electrostatic environment of carbohydrate pyrolysis, the DFT calculations determine how the kinetics of key glucose pyrolysis reactions are affected under sodium's influence. They provide an electronic-level basis to understand such effects that can be extrapolated to apply to other alkali and alkaline-earth metals and to additional carbohydrate decomposition reactions in similar reaction families. While the reaction network of glucose pyrolysis is too complex to allow direct comparison of the DFT and experimental results, this study provides the data required to build a microkinetic model of carbohydrate pyrolysis capable of verifying the computational results.

2. EXPERIMENTAL METHODS

Glucose was purchased from Fisher Scientific and had an ignition residue <0.002%, heavy metals <5.0 ppm, and iron <5.0 ppm, which were sufficiently low so as to eliminate the metal ion catalytic effect during pyrolysis.[42] For the impregnated glucose samples, the required amount of NaCl was measured in a beaker and then 1.0 g of glucose was added followed by 25 mL of methanol. With stirring, the mixture was completely dissolved and then the methanol was evaporated at 40 °C in an oven to yield a single solid.

The pyrolytic and analytical procedures have been thoroughly discussed in our previous work.[53] In short, a single-shot micropyrolyzer (Model 2020 iS, Frontier Laboratories, Japan) was used for the pyrolysis experiments. To perform an experiment, a deactivated stainless steel sample cup loaded with approximately 500 μg of sample was dropped into a quartz pyrolysis tube. The quartz tube was surrounded by a tubular furnace, which provided uniform heating and maintained the pyrolysis temperature of 500 °C used in this work. As demonstrated previously, maintaining a sample weight between 200 and 800 μg and particle size less than 75 μm ensured negligible heat transfer and mass transfer limitations.[42] Once generated, the volatile products were swept by helium gas into a Bruker 430-GC instrument through a deactivated needle.

dx.doi.org/10.1021/cs501125n | ACS Catal. 2015, 5, 192−202

For product identification, the GC was connected to a mass spectrometer (MS) (Saturn 2000), which used the electron ionization mode with a 10 μA emission current in the m/z range between 30 and 300. The mass spectra of the peaks were compared with standard spectra of chemical compounds within the NIST library database. The chemical identities were verified by running standards of the matching chemicals in the same GC-MS system and comparing their retention times with those of the glucose pyrolytic products.

After product identification, a flame ionization detector (FID) was substituted for the MS for product quantification. The FID was held at 250 °C with an air flow rate of 300 mL/min and hydrogen flow rate of 30 mL/min. The pure compounds used in product identification were also used in calibration of the FID results. Linear calibration curves (R^2 > 0.95), correlating the FID peak area with the standard concentration, were obtained by running four concentration levels for each pure standard. To quantify levoglucosan-furanose, 1,4:3,6-dianhydro-α-D-glucopyranose, and levoglucosenone, the calibration curve for levoglucosan-pyranose was used.

For CO and CO_2 quantification, the split line of the GC was connected to a De-Jaye gas analyzer equipped with an infrared detector. The concentrations of CO and CO_2 were recorded every 1 s, and thus the yields of CO and CO_2 could be calculated by summing the amount of gas generated over time using the known overall gas flow rate. The char yield was obtained by weighing the sample cup before and after pyrolysis using a Mettler Toledo microbalance with a sensitivity of ±1 μg.

3. COMPUTATIONAL METHODS

QM calculations were conducted using a methodology consistent with our recent modeling of neat glucose pyrolysis reactions.[53] Briefly, we employed Gaussian 09 rev C[60] with the M06-2X[61] functional and 6-311+G(2df,p) basis set,[62,63] specifying the "tight" optimization convergence criteria and "ultrafine" integration grids. The electrostatic environment of glucose pyrolysis was emulated using the PCM implicit solvent model[64] for ethanol. As noted in our previous work,[53] the dielectric constant of glucose has been reported to be 21.0 at 150 °C and is expected to be slightly greater at 500 °C.[65−67] We have previously validated that incorporation of implicit solvent effects in a system including a unipositive charge yields satisfactory model conformations consistent with simulations that explicitly include solvent molecules and differs from calculations performed purely in vacuo.[58] Natural population analysis and natural bond orbital (NBO)[68] analysis were performed using NBO 6.0.[69]

We explored the potential energy landscape of all stationary points to seek low free energy conformations. All local minima were verified to have zero imaginary frequencies. Transition states were verified to have exactly one imaginary frequency, and the intrinsic reaction coordinates were followed from each transition state to connect it with the correct local minima, using the Hessian-based Predictor−Corrector integration method.[70−73] As in our previous work,[53] frequencies were scaled with factors reported by Merrick et al.[74] for the M05-2X/6-311+G(2df,p) level of theory: 0.9663 for zero-point vibrational energy, 0.9444 for fundamental frequencies, 0.9168 for low frequencies (wavenumbers less than 260 cm^{-1}), 0.9297 for enthalpy calculations, and 0.9206 for entropy calculations. To obtain kinetic parameters, reaction rate coefficients were calculated at 100 K intervals between 300 and 1500 K using transition state theory[75] with a 1 M ideal solution as the standard state, and the results were fit to the Arrhenius equation. We focus on relative rate coefficients and on E_A in our comparison of reactions, since any inaccuracies in frequency calculations affect A more than E_A, and differences in reaction rate coefficients in a given reaction family are primarily due to differences in E_A. Thus, the relative rate coefficients among families are of greater importance than the absolute values.

4. RESULTS

4.1. Glucose Pyrolysis with NaCl. Figure 1 displays results of pyrolyzing glucose with varying amounts of NaCl, from 0 up

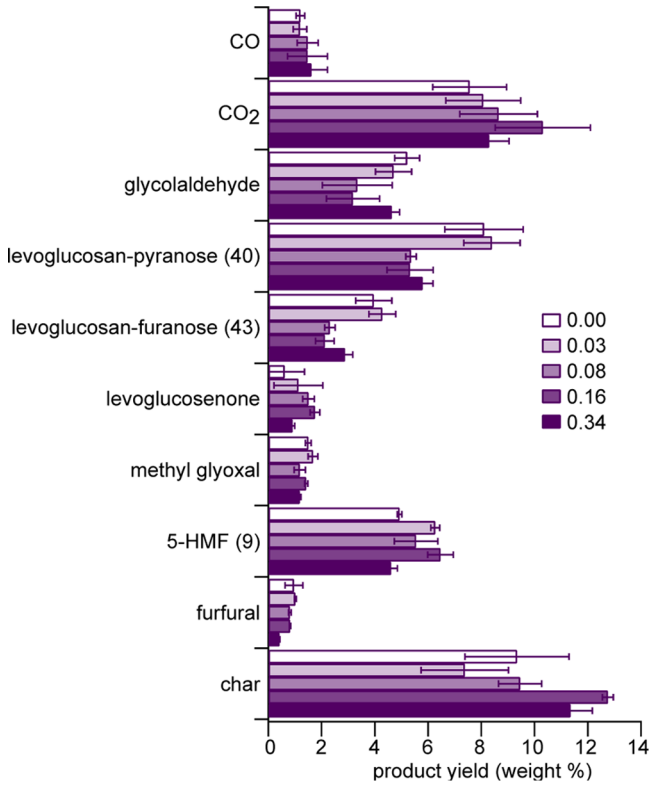

Figure 1. Key pyrolysis product yields of samples with between 0.00 and 0.34 mmol of NaCl per g of glucose. A full list of product yields is included in the Supporting Information. Numbers in parentheses correspond to numbers in Scheme 1.

to 2 wt % (0 mmol of NaCl/g of glucose to 0.34 mmol of NaCl/g of glucose). For clarity, products with less than 1 wt % yield in all cases were omitted from the figure; a full list of product yields is included in the Supporting Information.

The complex, nonmonotonic response of product yield to increasing NaCl loading is an outcome of the many competing reactions involved in carbohydrate pyrolysis,[23−25,29,30] and the various degrees to which the rate coefficients of these reactions can be affected, as discussed in the following section. While the effect of NaCl is less pronounced in glucose pyrolysis, the major trends previously reported for cellulose pyrolysis with NaCl are generally present. In the pyrolysis of glucose with NaCl, the yield of furans, such as 5-HMF, a major product from glucose pyrolysis, does not appear to significantly change with different NaCl loadings.[42] However, the presence of NaCl results in a decrease in levoglucosan and anhydrosugar yield

dx.doi.org/10.1021/cs501125n | ACS Catal. 2015, 5, 192−202

Scheme 1. Elementary Steps Included in This Study: (A) Conversion of β- and α-D-Glucose (1 and 2) to 5-HMF (9); (B) 1,2-Dehydration Reactions of Open D-Glucose (3); (C) 1,2-Dehydration Reactions of β-D-Glucose (1) to Cyclic Enols; (D) 1,2-Dehydration Reactions of α-D-Glucose (2) to Cyclic Enols; (E) 1,2-Dehydration Reactions of the *gem* Diol (17); (F) 1,2-Dehydration Reactions of the Carbaldehyde (7); (G) Conversion of β- and α-D-Glucose (1 and 2) to the Pyranose Form of Levoglucosan (40); (H) Conversion of Open D-Glucose (3) to the Furanose Form of Levoglucosan (43)

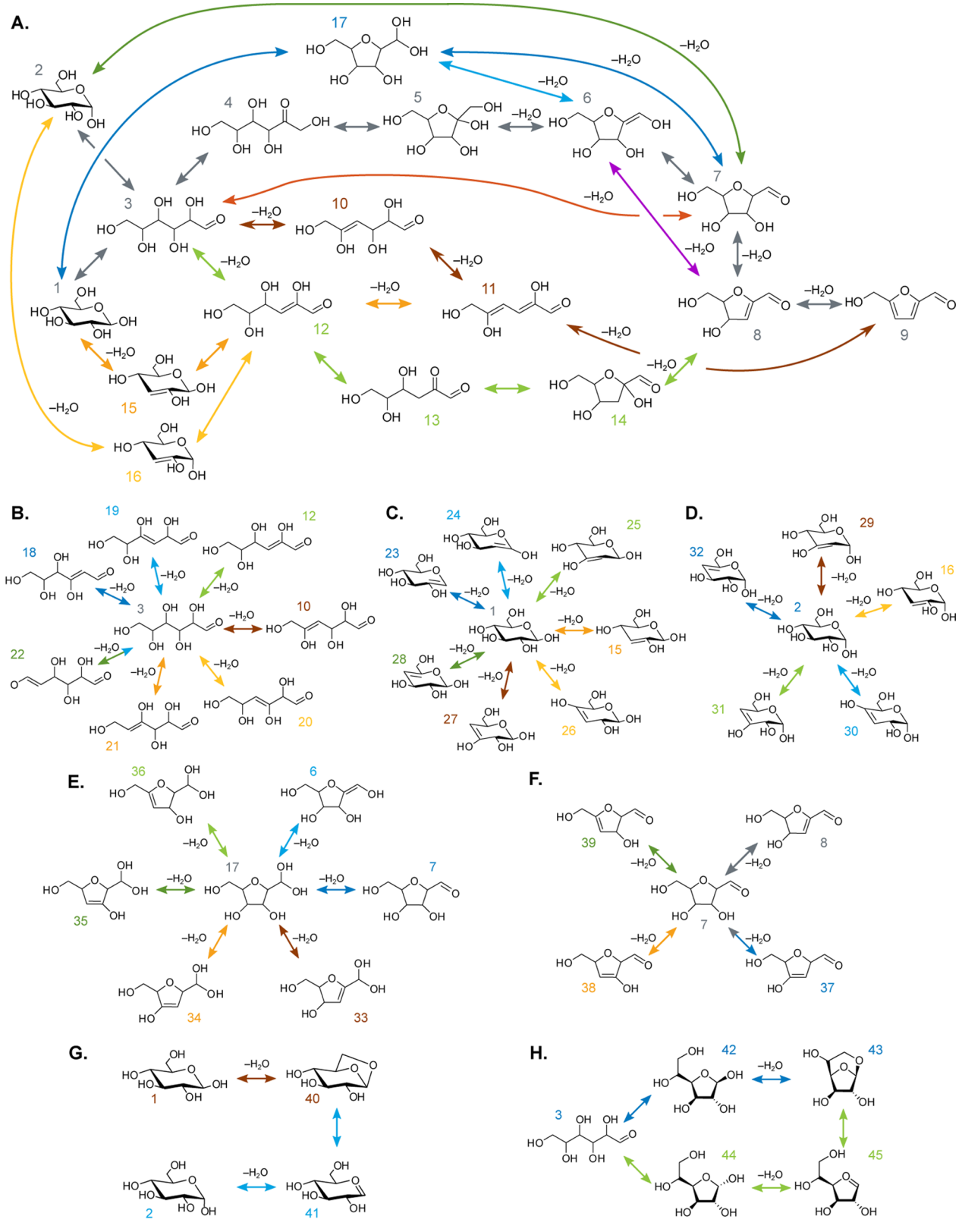

dx.doi.org/10.1021/cs501125n | ACS Catal. 2015, 5, 192−202

Table 1. Kinetic Parameters[a] for the Elementary Steps Shown in Scheme 1

reaction	forward direction with Na^+				reverse direction with Na^+			
	E_A	A	$k_{500\ °C}$	k_{Na^+}/k_{neat}	E_A	A	$k_{500\ °C}$	k_{Na^+}/k_{neat}
			Scheme 1A					
			Gray Path					
1 ↔ **3**	46.3	2.7×10^{14}	2.2×10	11.0	37.8	1.1×10^{13}	2.2×10^{2}	11.2
2 ↔ **3**	46.9	6.6×10^{13}	3.7	2.3	37.3	1.3×10^{12}	3.7×10	3.1
3 ↔ **4**	36.5	2.6×10^{12}	1.2×10^{2}	4.5	39.8	9.1×10^{11}	5.1	2.2
4 ↔ *β*-**5**	38.2	4.1×10^{11}	6.5	0.2	40.7	9.2×10^{12}	2.8×10	0.7
4 ↔ *α*-**5**	37.1	4.7×10^{11}	1.6×10	2.3	41.7	1.7×10^{13}	2.7×10	2.1
β-**5** ↔ **6** + H_2O	51.6	2.5×10^{13}	6.3×10^{-02}	0.5	36.4	5.1×10^{6}	2.6×10^{-4}	0.2
α-**5** ↔ **6** + H_2O	53.4	3.6×10^{14}	2.8×10^{-1}	7.7	36.1	4.7×10^{7}	2.9×10^{-3}	8.6
6 ↔ *trans*-**7**	62.6	2.9×10^{12}	5.8×10^{-6}	0.4	63.1	1.2×10^{11}	1.8×10^{-7}	0.6
trans-**7** ↔ **8** + H_2O	46.0	1.1×10^{11}	1.1×10^{-2}	7.0	46.0	3.6×10^{6}	3.6×10^{-7}	9.4
8 ↔ **9** + H_2O	57.4	2.3×10^{15}	1.4×10^{-1}	106.2	65.4	3.0×10^{8}	9.6×10^{-11}	113.5
			Purple Path					
6 ↔ **8** + H_2O	38.3	9.1×10^{12}	1.3×10^{2}	1.7	38.8	1.2×10^{7}	1.3×10^{-4}	3.5
			Brown Path					
3 ↔ **10** + H_2O	75.5	6.0×10^{15}	2.7×10^{-6}	1.9	65.6	4.9×10^{7}	1.4×10^{-11}	0.8
10 ↔ **11** + H_2O	54.5	8.6×10^{12}	3.3×10^{-03}	0.8	57.2	6.3×10^{6}	4.0×10^{-10}	3.6
11 ↔ **9** + H_2O	63.3	8.8×10^{6}	1.1×10^{-11}	0.0	63.3	8.8×10^{6}	1.1×10^{-11}	16.8
			Red Path					
3 → *cis*-**7** + H_2O	63.0	9.8×10^{13}	1.4×10^{-4}	1.9				
			Light Green Path					
3 ↔ **12** + H_2O	56.4	2.3×10^{13}	2.6×10^{-3}	0.6	53.0	3.0×10^{6}	2.9×10^{-9}	0.6
12 ↔ **13**	67.5	3.7×10^{13}	2.9×10^{-6}	3.5	66.1	1.0×10^{13}	2.0×10^{-6}	2.6
13 ↔ *β*-**14**	32.7	5.4×10^{11}	3.0×10^{2}	1.9	41.5	1.1×10^{14}	1.9×10^{2}	4.4
13 ↔ *α*-**14**	35.3	1.3×10^{12}	1.4×10^{2}	3.3	44.8	3.6×10^{14}	7.4×10	4.1
β-**14** ↔ **8** + H_2O	56.2	1.7×10^{14}	2.1×10^{-2}	15.1	43.2	5.2×10^{7}	3.1×10^{-5}	9.7
α-**14** ↔ **8** + H_2O	61.8	5.4×10^{14}	1.7×10^{-3}	15.8	48.1	1.2×10^{8}	3.1×10^{-6}	19.5
			Orange Path					
1 ↔ **15** + H_2O	70.8	2.1×10^{12}	2.0×10^{-8}	1.6	59.8	8.0×10^{5}	1.0×10^{-11}	2.0
15 ↔ **12**	42.3	9.3×10^{13}	1.0×10^{2}	12.4	41.5	1.3×10^{12}	2.4	9.4
12 ↔ **11** + H_2O	67.5	1.2×10^{15}	1.0×10^{-4}	28.4	63.7	5.6×10^{7}	5.4×10^{-11}	55.8
			Yellow Path					
2 ↔ **16** + H_2O	70.4	2.0×10^{12}	2.4×10^{-8}	3.2	59.2	5.9×10^{5}	1.1×10^{-11}	8.3
16 ↔ **12**	43.7	1.8×10^{13}	7.9	2.7	42.0	1.6×10^{11}	2.0×10^{-1}	1.3
			Blue Path					
1 ↔ **17**	72.7	1.5×10^{14}	4.0×10^{-7}	32.9	67.9	1.2×10^{13}	7.3×10^{-7}	18.9
17 ↔ *trans*-**7** + H_2O	40.9	2.6×10^{12}	7.3	1.5	27.2	1.2×10^{5}	2.5×10^{-3}	5.7
			Light Blue Path					
17 ↔ **6** + H_2O	67.1	1.1×10^{14}	1.1×10^{-5}	0.8	54.0	8.7×10^{7}	4.6×10^{-8}	0.8
			Dark Green Path					
2 ↔ *trans*-**7** + H_2O	63.6	5.9×10^{14}	6.0×10^{-4}	5.2	44.0	1.1×10^{6}	3.8×10^{-7}	14.8
			Scheme 1B					
3 ↔ **10** + H_2O	75.5	6.0×10^{15}	2.7×10^{-6}	1.9	65.6	4.9×10^{7}	1.4×10^{-11}	0.8
3 ↔ **12** + H_2O	56.4	2.3×10^{13}	2.6×10^{-3}	0.6	53.0	3.0×10^{6}	2.9×10^{-9}	0.6
3 ↔ **18** + H_2O	75.4	6.8×10^{14}	3.2×10^{-7}	15.0	76.2	2.9×10^{9}	8.4×10^{-13}	22.6
3 → **19** + H_2O	77.9	2.0×10^{15}	1.9×10^{-7}	1.1				
3 → **20** + H_2O	70.1	1.7×10^{14}	2.5×10^{-6}	2.7				
3 → **21** + H_2O	71.5	5.6×10^{14}	3.4×10^{-6}	1.1				
3 → **22** + H_2O	67.2	5.2×10^{14}	5.1×10^{-5}	9.7				
			Scheme 1C					
1 ↔ **15** + H_2O	70.8	2.1×10^{12}	2.0×10^{-8}	1.6	59.8	8.0×10^{5}	1.0×10^{-11}	2.0
1 → **23** + H_2O	59.0	8.2×10^{13}	1.6×10^{-3}	6.7				
1 → **24** + H_2O	80.5	5.8×10^{13}	9.8×10^{-10}	1.5				
1 → **25** + H_2O	76.5	1.0×10^{14}	2.3×10^{-8}	1.0				
1 → **26** + H_2O	78.5	1.9×10^{14}	1.2×10^{-8}	0.6				
1 → **27** + H_2O	75.2	6.7×10^{13}	3.5×10^{-8}	1.0				
1 → **28** + H_2O	75.1	1.5×10^{14}	8.3×10^{-8}	2.2				

dx.doi.org/10.1021/cs501125n | ACS Catal. 2015, 5, 192−202

Table 1. continued

reaction	forward direction with Na^+				reverse direction with Na^+			
	E_A	A	$k_{500\ °C}$	k_{Na^+}/k_{neat}	E_A	A	$k_{500\ °C}$	k_{Na^+}/k_{neat}
			Scheme 1D					
2 ↔ **16** + H_2O	70.4	2.0×10^{12}	2.4×10^{-8}	3.2	59.2	5.9×10^{5}	1.1×10^{-11}	8.3
2 → **29** + H_2O	74.9	2.7×10^{14}	1.7×10^{-7}	1.4				
2 → **30** + H_2O	79.0	5.5×10^{14}	2.5×10^{-8}	0.5				
2 → **31** + H_2O	75.5	4.1×10^{13}	1.8×10^{-8}	0.2				
2 → **32** + H_2O	74.1	2.1×10^{13}	2.3×10^{-8}	4.9				
			Scheme 1E					
17 ↔ **6** + H_2O	67.1	1.1×10^{14}	1.1×10^{-5}	0.8	54.0	8.7×10^{7}	4.6×10^{-8}	0.8
17 ↔ *trans*-**7** + H_2O	40.9	2.6×10^{12}	7.3	1.5	27.2	1.2×10^{5}	2.5×10^{-3}	5.7
17 → **33** + H_2O	67.2	2.1×10^{12}	2.1×10^{-7}	1.3				
17 → **34** + H_2O	71.1	7.1×10^{12}	5.4×10^{-8}	1.0				
17 → **35** + H_2O	70.5	7.6×10^{12}	8.8×10^{-8}	0.5				
17 → **36** + H_2O	69.7	2.1×10^{12}	4.0×10^{-8}	0.3				
			Scheme 1F					
trans-**7** ↔ **8** + H_2O	46.0	1.1×10^{11}	1.1×10^{-2}	7.0	46.0	3.6×10^{6}	3.6×10^{-7}	9.4
trans-**7** → **37** + H_2O	68.0	1.1×10^{12}	6.3×10^{-8}	0.8				
trans-**7** → **38** + H_2O	65.7	1.1×10^{12}	2.9×10^{-7}	2.1				
trans-**7** → **39** + H_2O	64.1	1.5×10^{11}	1.2×10^{-7}	1.7				
			Scheme 1G					
1 ↔ **40** + H_2O	47.4	4.2×10^{14}	1.7×10^{1}	52.3	42.2	1.2×10^{11}	1.4×10^{-1}	41.6
2 ↔ **41** + H_2O	77.0	3.2×10^{14}	5.5×10^{-8}	0.1	14.3	1.0×10^{7}	9.4×10^{2}	0.2
41 ↔ **40**	25.1	1.4×10^{11}	1.1×10^{4}	0.5	81.4	5.7×10^{14}	5.3×10^{-9}	0.5
			Scheme 1H					
3 ↔ **42**	33.6	1.6×10^{11}	5.0×10	2.7	39.5	5.5×10^{12}	3.8×10	1.5
42 ↔ **43** + H_2O	51.2	1.4×10^{14}	4.6×10^{-01}	2.1	37.3	1.1×10^{9}	2.9×10^{-02}	26.4
3 ↔ **44**	35.5	7.2×10^{11}	6.6×10	2.2	38.6	3.7×10^{12}	4.6×10	2.1
44 ↔ **45** + H_2O	69.1	3.7×10^{14}	1.1×10^{-5}	0.8	13.9	4.0×10^{8}	4.7×10^{4}	1.2
45 ↔ **43**	26.3	4.9×10^{11}	1.8×10^{4}	1.7	70.3	2.2×10^{13}	2.9×10^{-7}	8.1

[a] E_A values are given in kcal/mol; for unimolecular reactions, the units of A and k are s^{-1}; for bimolecular reactions, the units of A and k are $M^{-1}\ s^{-1}$.

and an increased yield of char, confirming that inorganic salts affect glucose pyrolysis. The alterations in the glucose pyrolysis product distribution are similar to those reported for cellulose pyrolysis with NaCl,[33−36,41,42,44] suggesting that understanding the effect of NaCl on glucose pyrolysis will be useful for understanding the effect for cellulose pyrolysis.

4.2. Effect of Na^+ on Key Glucose Pyrolysis Reaction Steps. Many key reactions in carbohydrate pyrolysis involve dehydration and isomerization.[23−25,29,30,49,52,76] In this work, we focus on an important subset of these reactions, namely those involved in the evolution of 5-HMF and levoglucosan, as well as a variety of competing decomposition reactions shown in Scheme 1, where each arrow represents an elementary step for which we have isolated transition states. Scheme 1A portrays competing reactions than can convert β-D-glucose (**1**) into 5-HMF (**9**), including via interconversion to α-D-glucose (**2**) through open D-glucose (**3**). The different colors correspond to different hypotheses of the most kinetically significant paths under pyrolysis conditions. The gray pathway represents an often-referenced pathway through D-fructose (**4**) and α-D-fructose (α-**5**) or β-D-fructose (β-**5**). Pathways in other colors represent alternative routes to 5-HMF, such as blue pathways, through a *gem* diol (**17**), and the purple step, bypassing a carbaldehyde (**7**) in the "via fructose" (gray) pathway.[53] Examining this variety of pathways allows determination of whether the same pathways will be kinetically dominant upon inclusion of inorganic salts. The reactions in Scheme 1B further elucidate the effect of Na^+ on competing reactions, in this case the full complement of open D-glucose (**3**) 1,2-dehydration reactions, of which two such reactions are invoked in glucose to 5-HMF pathways. Similarly, Scheme 1C explores other 1,2-dehydration reactions of β-D-glucose (**1**) to cyclic enols, beyond the one option invoked in Scheme 1A. There are fewer 1,2-dehydration reactions of α-D-glucose (**2**) to cyclic enols, shown in Scheme 1D, in comparison to Scheme 1C, due to the differing orientation of the anomeric hydroxyl group. Scheme 1E,F further explores reactions that can compete with those in Scheme 1A, specifically the full complement of 1,2-dehydration reactions of the *gem* diol (**17**) and carbaldehyde (**7**), respectively. Scheme 1G presents the mechanisms for producing the pyranose form of levoglucosan (1,6-anhydro-β-D-glucopyranose; **40**) directly from β-D-glucose (**1**) or from α-D-glucose (**2**) via a carbene intermediate (**41**). Finally, Scheme 1H presents the mechanisms for producing the furanose form of levoglucosan (1,6-anhydro-β-D-glucofuranose; **43**) from β-D-glucofuranose (**42**) or α-D-glucofuranose (**44**) by means of a carbene intermediate (**45**). Either furanose form of glucose can be formed by ring closure of D-glucose (**3**), which in turn can be formed by ring opening of α- or β-D-glucose, as shown in Scheme 1A. The findings for the reactions in this study can be extrapolated to other carbohydrate decomposition reactions according to the reaction family approach.[77]

We recently determined the kinetic parameters for each of these steps in the absence of any catalyst.[53] In the present work, we determine how the presence of Na^+ catalyzes these reactions. Some reactions found to be kinetically insignificant in the previous study were not included in this study, such as

dx.doi.org/10.1021/cs501125n | ACS Catal. 2015, 5, 192−202

conversion of **6** to **8** via a *cis*-**7** intermediate. For that path, the route through *cis*-**7** would not be competitive with conversion via *trans*-**7** even if Na^+ increased the rate coefficients by more than 5 orders of magnitude. Such an increase would be far beyond the maximum increase of 2 orders of magnitude for the reactions included in the present study. Similarly, we did not include several reverse reactions that would require water to act as a reactant, as they are expected to be kinetically insignificant due to a very low concentration of water, which readily volatilizes under fast pyrolysis conditions. The present work maintains the same numbering scheme as used in the neat glucose decomposition study to aid comparison of results.

As detailed in another recent work,[58] there are a profusion of low-energy conformations of glucose with a sodium ion, resulting from the combination of carbohydrate rotamers with the multiple favorable positions for the ion to associate with the carbohydrate. We repeated our search for low-energy conformations of α- and β-D-glucose bound with Na^+, this time employing implicit ethanol as the solvent to mimic the glucose pyrolysis electrostatic environment. The results were similar to those previously reported using implicit water as the solvent, with the lowest-energy conformations of α-D-glucose-and β-D-glucose-Na^+ adopting chair orientations for the ring geometry.[58] A similar investigation of low-energy conformations was required for each stable point, investigating the degrees of freedom due to exocyclic group rotations and various positions of the sodium ion. Additionally, in many cases, the lowest energy conformation of a transition state employed a puckered conformation[28] for the ring geometry. Images of the three-dimensional structures of the lowest free energy conformation found for each stable point are included in the Supporting Information, as are the atomic Cartesian coordinates, electronic energies, enthalpies, and free energies. The presence of a sodium ion did not lead us to fundamentally different reaction mechanisms; the most energetically favorable mechanisms obtained were for concerted bond cleavage and formation, as found with neat glucose decomposition, rather than favoring heterolytic or homolytic cleavage. However, the kinetic parameters were significantly perturbed, as shown in Table 1 in the ratio of the rate coefficients at 500 °C for the elementary step when sodium is present to when it is absent (k_{Na^+}/k_{neat}). We used the lowest free-energy conformations to calculate kinetic parameters, corresponding to the conformations that provide the largest rate coefficient at 500 °C, which do not always correspond to the lowest E_A value. For the set of reactions in this study, the effect of the sodium ion ranges from increasing the rate coefficient by 2 orders of magnitude to decreasing it by more than 2 orders of magnitude, with about 70% of the reactions catalyzed by Na^+, about 25% inhibited by Na^+, and the remainder showing virtually no effect on the rate coefficient. The average value of the k_{Na^+}/k_{neat} ratio is 5.9, with a 14.0 standard deviation. The positive mean value is consistent with the experimentally observed overall increased rate of reaction when inorganic salts are present,[33,40] while the large standard deviation reflects a broad range of effects, consistent with the observed changes in relative product yields.

Given the diversity of the effect that Na^+ has on different reactions and even reactions in the same family, we sought to rationalize these effects on the basis of other information available from the high-level electronic structure calculations completed in this study. The Cartesian coordinates and three-dimensional images of the stable points presented in the Supporting Information in this paper and our previous work without ions[53] show that the lowest-energy conformations with sodium present are typically quite similar to the neat conformations, often employing only different orientations of hydrogen atoms to accommodate the sodium ion. Some of the cyclic molecules adopt a different orientation for the hydroxymethyl group, and it is quite common for the backbone structures of the noncyclic molecules to adopt a fairly linear alignment of the carbon backbone when no ions are present and a more curved alignment when Na^+ is present.

Figures 2 and 3 compare selected reactants and transition states, respectively, in the absence or presence of a sodium ion. The noted interatomic distances and partial charges are for the atoms involved in the reaction centers for the reactions shown in Figure 3. As was the case with α- and β-D-glucose with implicit water,[58] the presence of a sodium ion did not significantly perturb reactant structures, as shown in Figure 2. In these examples, bond lengths were perturbed by no more than 0.01 Å (overall RMSD of 0.00 Å for values shown), implying little effect on bond strength, and NBO partial charge differences of no more than 0.062 au (RMSD of 0.016 au for the values shown, omitting the Na^+ partial charge).

Despite minimal changes to reactant conformations, notable changes were observed in the transition state structures, as demonstrated in Figure 3. Comparing the partial charges of the neat reactants and neat transition states reveals evolution of charge separation at the reaction centers of the transition states, illuminating why the sodium ion interacts more intimately with the transition state structures. Accordingly, the perturbations on NBO partial charges are larger than those for the reactants, with differences in NBO partial charges in some cases exceeding 0.1 au (overall RMSD of 0.048 au for values shown, omitting the Na^+ partial charge) and the distances between atoms in the reaction centers can differ by more than 0.2 Å (RMSD of 0.08 Å for values shown). Not surprisingly, the transition state that displays the most perturbed structural parameters (the transition state for **8** → **9**, Figure 3H) corresponds to the reaction with the rate coefficient most significantly altered by the presence of Na^+ (k_{Na^+}/k_{neat} = 106). In this case, Na^+ stabilizes an "exploded" transition state, with the leaving O4 2.59 Å from C4, an increase of 0.20 Å, and 0.14 Å farther from the hydrogen it will abstract.

In the **8** → **9** transition state, the sodium ion is located near the reaction center. However, adjacency of the cation is not required to have a large effect on the reaction rate, as shown in Figure 3E. In this transition state leading from β-D-glucose to levoglucosan (**1** → **40** + H_2O), the Na^+ is not adjacent to the reaction center, yet its presence increases the rate coefficient 52 times. As verified by NBO analysis, the O3 hydroxyl group strongly stabilizes the transition state both with and without Na^+ present. In the transition state with Na^+ present, the ion is closest to O3 (2.25 Å apart) and increases the O3 hydroxyl group stabilizing interactions with the reaction center, according to NBO second-order perturbation theory. The effect of the ion is further evidenced by changes to the atomic structure: when Na^+ is present, the O3−HO3 bond elongates from 1.03 to 1.06 Å and the HO3−O6 distance shortens from 1.48 to 1.38 Å. Clearly, there are multiple ways that metal ions can stabilize transition states, and the mechanism is not limited to direct interaction of the ion with atoms in the reaction center.

Conversely to Figure 3E, showing that Na^+ resulting in little change in reaction center distances and partial charges do not necessarily correspond to little effect on rate coefficient, Figure

dx.doi.org/10.1021/cs501125n | ACS Catal. 2015, 5, 192−202

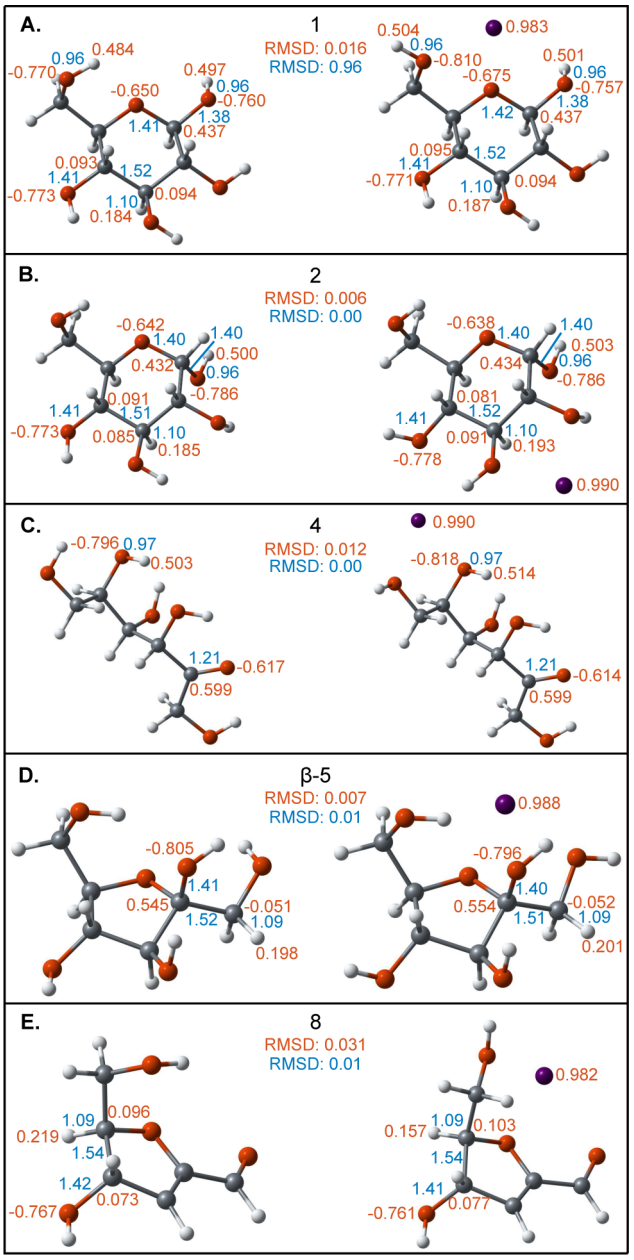

Figure 2. Comparisons of conformation, key distances, and partial charges in the absence of a sodium ion (molecule on left in each pair; neat structures from Mayes et al.[53]) or in its presence (molecule on right), for the following selected reactants (identified by index numbers corresponding to those in Scheme 1): (A) β-D-glucose (**1**); (B) α-D-glucose (**2**); (C) D-fructose (**4**); (D) β-D-fructose (β-**5**); (E) dihydrofuran precursor (**8**) to 5-HMF. Numbers in blue indicate distances in Å, including the RMSD of the distances shown, and numbers in red indicate NBO partial charges in au, including the RMSD of the labeled partial charges (Na^+ partial charges not included in the RMSD).

3C shows that Na^+ perturbing reaction center distances and partial charges does not necessarily correspond to altered rate coefficients: several distances at the reaction center of the dehydration **1** → **27** + H_2O are perturbed by more than 0.1 Å while the rate coefficient is unaffected. As a further illustration of range of sodium ion effects, the transition state structures for the dehydration reaction β-**5** → **6** + H_2O are virtually identical with and without Na^+ present, while the rate coefficient is depressed by Na^+ (Figure 3G).

Figure 3A-D compares the effect of Na^+ on the same reaction with either β- or α-D-glucose (**1** or **2**). The k_{Na^+}/k_{neat} value of **11** for the ring-opening reaction **1** → **3** is greater than that for **2** → **3**, which has a k_{Na^+}/k_{neat} value of 2, and the value of k_{Na^+}/k_{neat} for the dehydration reaction **1** → **27** + H_2O is unaffected while that for **2** → **31** + H_2O is decreased. For these pairs, the sodium ion is located at different positions, attributable to the differences in stereochemistry of the anomers and emphasizing the role of stereochemistry in how ions differently affect different transition state structures.

5. DISCUSSION AND CONCLUSIONS

Heterolytic cleavage had been proposed to explain the drastic change in product yields during the pyrolysis of cellulose due to the presence of inorganic salts such as NaCl.[35,42,45,48,78,79] The finding that concerted reactions likely dominate at pyrolysis temperatures[26] reopens the question of why and how the presence of inorganic salts perturbs pyrolysis product yields. In this work, we showed that, even for concerted reactions, metal ions can perturb rate coefficients by more than 1 order of magnitude by interaction with charge-separated transition states, a classic catalytic or inhibitory mechanism.[80−82] The rate coefficient for the majority of the reaction steps increased, consistent with the experimental observation of increased reaction rate when inorganic salts are present.[33,40] Significantly, not all rate coefficients for the reactions studied increase due to the presence of Na^+, and the effect varies in magnitude. This provides an important extension to the earlier work by Nimlos et al.[52] by highlighting that the effect of the metal ion depends not just on reaction type (e.g., dehydration) but also on the stereochemistry at and around the reaction center. While this study did not examine every elementary step important in glucose pyrolysis, the range of isomerization and dehydration steps explored provides a basis for extrapolating kinetic information on other important, similar elementary steps—such as those involved in fragmentation reactions to CO, CO_2, and glycolaldehyde—using a reaction family approach.[77]

Perturbations to rate coefficients for the same reaction network, rather than altering the reaction network, are consistent with the observation of the same products from pyrolysis of neat glucose and glucose with NaCl present, but different product yields. Polysaccharide pyrolysis involves a complex reaction network comprised of many more reactions than those considered here,[23−25,29−31] and the relative rates of many competing reactions ultimately determine product yields. For example, while the rate of levoglucosan formation from β-D-glucose is increased by Na^+ to a greater extent than the ion increases the rate of β-D-glucose ring opening, the rate coefficient of ring opening remains greater in magnitude. A microkinetic model, which incorporates the elementary steps and kinetic parameters to determine species concentration over time, is required to quantitatively evaluate the accuracy of the DFT results. Importantly, this study presents kinetic parameters required for such a microkinetic model, allowing extension of microkinetic models of pure polysaccharide pyrolysis to include this important component of natural biomass. Additionally, it provides an important framework for understanding the effect of inorganic salts on the reaction network, namely the interaction of ions with charge separation that evolves at the transition state structures.

dx.doi.org/10.1021/cs501125n | ACS Catal. 2015, 5, 192−202

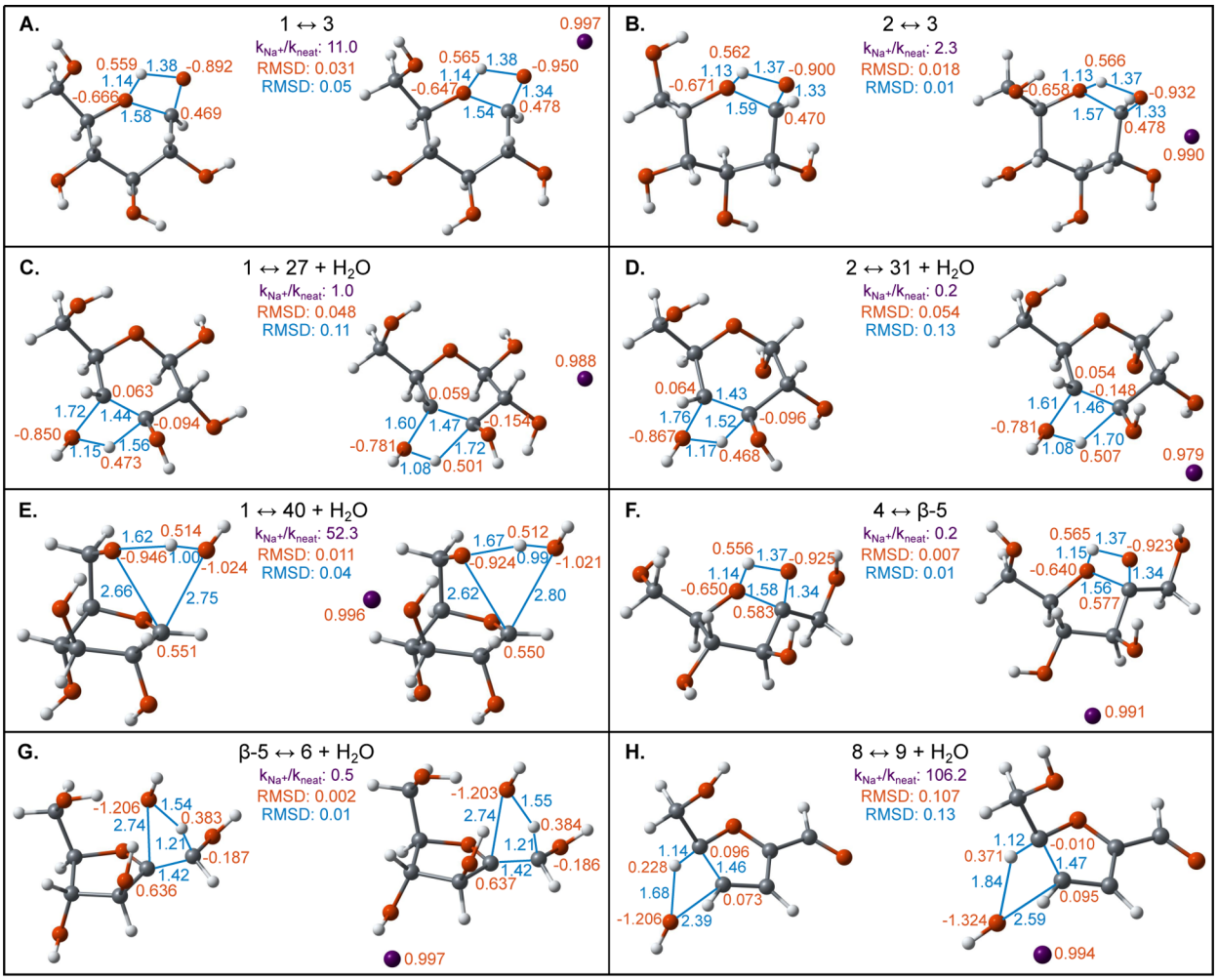

Figure 3. Comparisons of conformations, key distances, and partial charges in the absence of a sodium ion (molecule on left in each pair; neat structures from Mayes et al.[53]) or in its presence (molecule on right), for the following selected transition states: (A) ring opening of *β*-D-glucose (**1**) to D-glucose (**3**); (B) ring opening of *α*-D-glucose (**2**) to D-glucose (**3**); (C) dehydration of *β*-D-glucose (**1**) to a cyclic enol (**27**); (D) dehydration of *α*-D-glucose (**2**) to a cyclic enol (**31**); (E) dehydration of *β*-D-glucose (**1**) to levoglucosan (**40**); (F) ring closing of D-fructose (**4**) to *β*-D-fructose (*β*-**5**); (G) dehydration of *β*-D-fructose (*β*-**5**) to an enol (**6**); (H) dehydration of a dihydrofuran (**8**) to 5-HMF (**9**). Numbers in blue indicate distances in Å, and numbers in red indicate NBO partial charges in au. For each transition state, the k_{Na^+}/k_{neat} values from Table 1 are listed, as well as the RMSD values for the labeled distances (RMSD in blue) and labeled partial charges (RMSD values in red, omitting Na^+ partial charges).

■ ASSOCIATED CONTENT

Supporting Information

The following file is available free of charge on the ACS Publications website at DOI: 10.1021/cs501125n.

Three-dimensional images, atomic coordinates, electronic energies, enthalpies, and free energies for all structures (PDF)

■ AUTHOR INFORMATION

Corresponding Authors

*E-mail for B.H.S.: bshanks@iastate.edu.
*E-mail for L.J.B.: broadbelt@northwestern.edu.

Notes

The authors declare no competing financial interest.

■ ACKNOWLEDGMENTS

This work was supported by the National Advanced Biofuels Consortium (NABC), which is funded by the Department of Energy (DOE) Office of Energy Efficiency and Renewable Energy through the Office of Biomass Program, grant number DE-EE0003044. This research used computational resources of the National Energy Research Scientific Computing Center, which is supported by the Office of Science of the U.S. DOE under Contract No. DE-AC02-05CH11231, the NREL Computational Sciences Center, which is supported by the DOE Office of EERE under Contract No. DE-AC36-08GO28308, and the San Diego Supercomputing Center, which is supported under the NSF XSEDE Grant MCB090159. The authors thank Glen A. Ferguson for valuable discussions and Chris Mayes for helpful scripts. H.B.M. was supported by a DOE Computational Science Graduate Fellowship (CSGF), which is provided under grant number DE-FG02-97ER25308, and the ARCS Foundation Inc., Chicago Chapter.

■ REFERENCES

(1) Huber, G. W.; Iborra, S.; Corma, A. *Chem. Rev.* **2006**, *106*, 4044–4098.

(2) Ragauskas, A. J.; Williams, C. K.; Davison, B. H.; Britovsek, G.; Cairney, J.; Eckert, C. A.; Frederick, W. J., Jr.; Hallett, J. P.; Leak, D. J.;

Liotta, C. L.; Mielenz, J. R.; Murphy, R.; Templer, R.; Tschaplinski, T. *Science* **2006**, *311*, 484−489.
(3) Pauly, M.; Keegstra, K. *Plant J.* **2008**, *54*, 559−568.
(4) Alonso, D. M.; Bond, J. Q.; Dumesic, J. A. *Green Chem.* **2010**, *12*, 1493−1513.
(5) Chundawat, S. P.; Beckham, G. T.; Himmel, M. E.; Dale, B. E. *Annu. Rev. Chem. Biomol. Eng.* **2011**, *2*, 121−145.
(6) Sheldon, R. A. *Green Chem.* **2014**, *16*, 950−963.
(7) Evans, R. J.; Milne, T. A. *Energy Fuels* **1987**, *1*, 311−319.
(8) Bridgwater, A. V.; Peacocke, G. V. C. *Renew. Sust. Energy Rev.* **2000**, *4*, 1−73.
(9) Serrano-Ruiz, J. C.; Dumesic, J. A. *Energy Environ. Sci.* **2011**, *4*, 83−99.
(10) Czernik, S.; Bridgwater, A. *Energy Fuels* **2004**, *18*, 590−598.
(11) Branca, C.; Di Blasi, C.; Elefante, R. *Energy Fuels* **2006**, *20*, 2253−2261.
(12) Mohan, D.; Pittman, C. U.; Steele, P. H. *Energy Fuels* **2006**, *20*, 848−889.
(13) Ringer, M.; Putsche, V.; Scahill, J. *Large-Scale Pyrolysis Oil Production: A Technology Assessment and Economic Analysis*; National Renewable Energy Laboratory: Golden, CO, 2006.
(14) Di Blasi, C. *Prog. Energy Combust. Sci.* **2008**, *34*, 47−90.
(15) Briodo, A.; Nelson, M. A. *Combust. Flame* **1975**, *24*, 263−268.
(16) Bradbury, A. G. W.; Sakai, Y.; Shafizadeh, F. J. *Appl. Polym. Sci.* **1979**, *23*, 3271−3280.
(17) Ranzi, E.; Cuoci, A.; Faravelli, T.; Frassoldati, A.; Migliavacca, G.; Pierucci, S.; Sommariva, S. *Energy Fuels* **2008**, *22*, 4292−4300.
(18) Authier, O.; Ferrer, M.; Khalfi, A.-E.; Lédé, J. *Int. J. Chem. Reactor Eng.* **2010**, *8*, A78.
(19) Lin, T.; Goos, E.; Riedel, U. *Fuel Process. Technol.* **2013**, *115*, 246−253.
(20) Patwardhan, P. R.; Satrio, J. A.; Brown, R. C.; Shanks, B. H. *J. Anal. Appl. Pyrolysis* **2009**, *86*, 323−330.
(21) Patwardhan, P. R.; Dalluge, D. L.; Shanks, B. H.; Brown, R. C. *Bioresour. Technol.* **2011**, *102*, 5265−5269.
(22) Paulsen, A. D.; Mettler, M. S.; Dauenhauer, P. J. *Energy Fuels* **2013**, *27*, 2126−2134.
(23) Paine, J. B., III; Pithawalla, Y. B.; Naworal, J. D. *J. Anal. Appl. Pyrolysis* **2008**, *82*, 10−41.
(24) Paine, J. B., III; Pithawalla, Y. B.; Naworal, J. D. *J. Anal. Appl. Pyrolysis* **2008**, *82*, 42−69.
(25) Paine, J. B., III; Pithawalla, Y. B.; Naworal, J. D. *J. Anal. Appl. Pyrolysis* **2008**, *83*, 37−63.
(26) Mayes, H. B.; Broadbelt, L. J. *J. Phys. Chem. A* **2012**, *116*, 7098−7106.
(27) Seshadri, V.; Westmoreland, P. R. *J. Phys. Chem. A* **2012**, *116*, 11997−12013.
(28) Mayes, H. B.; Broadbelt, L. J.; Beckham, G. T. *J. Am. Chem. Soc.* **2014**, *136*, 1008−1022.
(29) Vinu, R.; Broadbelt, L. J. *Energy Environ. Sci.* **2012**, *5*, 9808−9826.
(30) Zhou, X.; Nolte, M. W.; Mayes, H. B.; Shanks, B. H.; Broadbelt, L. J. *Ind. Eng. Chem. Res.* **2014**, *53*, 13274−13289.
(31) Zhou, X.; Nolte, M. W.; Shanks, B. H.; Broadbelt, L. J. *Ind. Eng. Chem. Res.* **2014**, *53*, 13290−13301.
(32) Shafizadeh, F. *J. Anal. Appl. Pyrolysis* **1982**, *3*, 283−305.
(33) Sekiguchi, Y.; Shafizadeh, F. *J. Appl. Polym. Sci.* **1984**, *29*, 1267−1286.
(34) Evans, R. J.; Milne, T. A. *Energy Fuels* **1987**, *1*, 123−137.
(35) Richards, G. N. *J. Anal. Appl. Pyrolysis* **1987**, *10*, 251−255.
(36) Várhegyi, G.; Antal, M. J., Jr.; Szekely, T.; Till, F.; Jakab, E. *Energy Fuels* **1988**, *2*, 267−272.
(37) Piskorz, J.; Radlein, D. S. A. G.; Scott, D. S.; Czernik, S. *J. Anal. Appl. Pyrolysis* **1989**, *16*, 127−142.
(38) Ponder, G. R.; Richards, G. N. *Carbohydr. Res.* **1993**, *244*, 341−359.
(39) Antal, M. J., Jr.; Varhegyi, G. *Ind. Eng. Chem. Res.* **1995**, *34*, 703−717.
(40) Sanders, E. B.; Goldsmith, A. I.; Seeman, J. I. *J. Anal. Appl. Pyrolysis* **2003**, *66*, 29−50.
(41) Shimada, N.; Kawamoto, H.; Saka, S. *J. Anal. Appl. Pyrolysis* **2008**, *81*, 80−87.
(42) Patwardhan, P. R.; Satrio, J. A.; Brown, R. C.; Shanks, B. H. *Bioresour. Technol.* **2010**, *101*, 4646−4655.
(43) Shaik, S. M.; Sharratt, P. N.; Tan, R. B. *J. Anal. Appl. Pyrolysis* **2013**, *104*, 234−242.
(44) Yu, Y.; Liu, D.; Wu, H. *Energy Fuels* **2014**, *28*, 245−253.
(45) Ponder, G. R.; Richards, G. N.; Stevenson, T. T. *J. Anal. Appl. Pyrolysis* **1992**, *22*, 217−229.
(46) Scott, D. S.; Paterson, L.; Piskorz, J.; Radlein, D. *J. Anal. Appl. Pyrolysis* **2001**, *57*, 169−176.
(47) Richards, G. N.; Zheng, G. J. *Anal. Appl. Pyrolysis* **1991**, *21*, 133−146.
(48) Ponder, G. R.; Richards, G. N. *Carbohydr. Res.* **1993**, *244*, 27−47.
(49) Lédé, J. *J. Anal. Appl. Pyrolysis* **2012**, *94*, 17−32.
(50) Julien, S.; Chornet, E.; Tiwari, P. K.; Overend, R. P. *J. Anal. Appl. Pyrolysis* **1991**, *19*, 81−104.
(51) Saddawi, A.; Jones, J. M.; Williams, A. *Fuel Process. Technol.* **2012**, *104*, 189−197.
(52) Nimlos, M. R.; Blanksby, S. J.; Ellison, G. B.; Evans, R. J. *J. Anal. Appl. Pyrolysis* **2003**, *66*, 3−27.
(53) Mayes, H. B.; Nolte, M. W.; Beckham, G. T.; Shanks, B. H.; Broadbelt, L. J. *ACS Sustainable Chem. Eng.* **2014**, *2*, 1461−1473.
(54) Radlein, D. S. T. A. G.; Grinshpun, A.; Piskorz, J.; Scott, D. S. *J. Anal. Appl. Pyrolysis* **1987**, *12*, 39−49.
(55) Piskorz, J.; Majerski, P.; Radlein, D.; Vladars-Usas, A.; Scott, D. S. *J. Anal. Appl. Pyrolysis* **2000**, *56*, 145−166.
(56) Wang, S.; Guo, X.; Liang, T.; Zhou, Y.; Luo, Z. *Bioresour. Technol.* **2012**, *104*, 722−728.
(57) Mettler, M. S.; Paulsen, A. D.; Vlachos, D. G.; Dauenhauer, P. J. *Green Chem.* **2012**, *14*, 1284−1288.
(58) Mayes, H. B.; Tian, J.; Nolte, M. W.; Shanks, B. H.; Beckham, G. T.; Gnanakaran, S.; Broadbelt, L. J. *J. Phys. Chem. B* **2014**, *118*, 1990−2000.
(59) Paine, J. B., III; Pithawalla, Y. B.; Naworal, J. D.; Thomas, C. E., Jr. *J. Anal. Appl. Pyrolysis* **2007**, *80*, 297−311.
(60) Frisch, M. J.; Trucks, G. W.; Schlegel, H. B.; Scuseria, G. E.; Robb, M. A.; Cheeseman, J. R.; Scalmani, G.; Barone, V.; Mennucci, B.; Petersson, G. A.; Nakatsuji, H.; Caricato, M.; Li, X.; Hratchian, H. P.; Izmaylov, A. F.; Bloino, J.; Zheng, G.; Sonnenberg, J. L.; Hada, M.; Ehara, M.; Toyota, K.; Fukuda, R.; Hasegawa, J.; Ishida, M.; Nakajima, T.; Honda, Y.; Kitao, O.; Nakai, H.; Vreven, T.; Montgomery, J. A.; Peralta, J. E.; Ogliaro, F.; Bearpark, M.; Heyd, J. J.; Brothers, E.; Kudin, K. N.; Staroverov, V. N.; Kobayashi, R.; Normand, J.; Raghavachari, K.; Rendell, A.; Burant, J. C.; Iyengar, S. S.; Tomasi, J.; Cossi, M.; Rega, N.; Millam, J. M.; Klene, M.; Knox, J. E.; Cross, J. B.; Bakken, V.; Adamo, C.; Jaramillo, J.; Gomperts, R.; Stratmann, R. E.; Yazyev, O.; Austin, A. J.; Cammi, R.; Pomelli, C.; Ochterski, J. W.; Martin, R. L.; Morokuma, K.; Zakrzewski, V. G.; Voth, G. A.; Salvador, P.; Dannenberg, J. J.; Dapprich, S.; Daniels, A. D.; Farkas; Foresman, J. B.; Ortiz, J. V.; Cioslowski, J.; Fox, D. J. *Gaussian 09 Revision C.01*; Gaussian, Inc.: Wallingford, CT, 2010.
(61) Zhao, Y.; Truhlar, D. G. *Theor. Chem. Acc.* **2008**, *120*, 215−241.
(62) Krishnan, R.; Binkley, J. S.; Seeger, R.; Pople, J. A. *J. Chem. Phys.* **1980**, *72*, 650−654.
(63) Frisch, M. J.; Pople, J. A.; Binkley, J. S. *J. Chem. Phys.* **1984**, *80*, 3265−3269.
(64) Tomasi, J.; Mennucci, B.; Cammi, R. *Chem. Rev.* **2005**, *105*, 2999−3093.
(65) Cattoir, F. R.; Parks, G. S. *J. Phys. Chem.* **1929**, *33*, 879−882.
(66) Chan, R. K.; Pathmanathan, K.; Johari, G. P. *J. Phys. Chem.* **1986**, *90*, 6358−6362.
(67) Calkins, C. R. *TAPPI J.* **1950**, *33*, 278−285.
(68) Glendening, E. D.; Landis, C. R.; Weinhold, F. *WIREs Comput. Mol. Sci.* **2012**, *2*, 1−42.

(69) Glendening, E.; Badenhoop, J. K. ; Reed, A. E. ; Carpenter, J. E. ; Bohmann, J. A. ; Morales, C. M. ; Landis, C. R. ; Weinhold, F. *NBO 6.0*; Theoretical Chemistry Institute: Madison, WI, 2013.
(70) Hratchian, H. P.; Schlegel, H. B. *J. Chem. Phys.* **2004**, *120*, 9918−9924.
(71) Hratchian, H. P. ; Schlegel, H. B. In *Theory and Applications of Computational Chemistry: The First Forty Years*; Dykstra, C. E., Frenking, G., Kim, K. S., Scuseria, G. , Eds.; Elsevier Science: Elsevier, Amsterdam, 2005; pp 195−249.
(72) Hratchian, H. P.; Schlegel, H. B. *J. Chem. Theory Comput.* **2005**, *1*, 61−69.
(73) Collins, M. A. *Theor. Chem. Acc.* **2002**, *108*, 313−324.
(74) Merrick, J. P.; Moran, D.; Radom, L. *J. Phys. Chem. A* **2007**, *111*, 11683−11700.
(75) Moore, J. W. ; Pearson, R. G. *Kinetics and Mechanism*, 3rd ed.; Wiley: New York, 1981; pp 159−172.
(76) Mettler, M. S.; Vlachos, D. G.; Dauenhauer, P. J. *Energy Environ. Sci.* **2012**, *5*, 7797−7809.
(77) Broadbelt, L. J.; Pfaendtner, J. *AIChE J.* **2005**, *51*, 2112−2121.
(78) Yang, C.-y.; Lu, X.-s.; Lin, W.-g.; Yang, X.-m.; Yao, J.-z. *Chem. Res. Chinese U.* **2006**, *22*, 524−532.
(79) Mamleev, V.; Bourbigot, S.; Le Bras, M.; Yvon, J. *J. Anal. Appl. Pyrolysis* **2009**, *84*, 1−17.
(80) Pauling, L. *Chem. Eng. News* **1946**, *24*, 1375−1377.
(81) Herschlag, D.; Jencks, W. P. *J. Am. Chem. Soc.* **1990**, *112*, 1942−1950.
(82) Pregel, M. J.; Dunn, E. J.; Nagelkerke, R.; Thatcher, G. R. J.; Buncel, E. *Chem. Soc. Rev.* **1995**, *24*, 449−455.